Evaluation of Alternate Materials for Organic/Inorganic Tunneling Diodes for Efficient, Water-Free and Flexible Organic Tandem Solar Cells

HONORS THESIS

Presented in Partial Fulfillment of the Requirements for Graduation with Honors Research Distinction in the Degree Bachelor of Science in the Undergraduate Colleges of The Ohio State University

By

Shloka Raghavan

Undergraduate Program in Electrical and Computer Engineering

The Ohio State University

2015

Thesis Committee:

Paul R. Berger, Advisor

George Valco

Abstract

Multi-junction Solar Cells are fabricated with multiple PN junctions in order to absorb light more efficiently than traditional solar cells. However, by stacking each of the multiple PN junctions in the solar cells to absorb different portions of the sun's spectrum, parasitic resistances are formed between each stacked PN junction due to polarity mismatches that reduces collection efficiencies. The problem that this research addresses is the need to develop flexible and robust tunneling junctions, which are a critical element in fabricating these flexible solar cells.

The purpose of the current research is to evaluate staggered junction candidates for the metal oxide and organic semiconductor in the fabrication of polymer tunneling diodes. This research study was prompted by prior research by Prof. Berger's group at Ohio State that demonstrated the feasibility to fabricate polymer based tunnel diodes using a thin metal oxide (TiO_2) and a conjugated polymer, Poly[2-methoxy-5-(2-ethylhexyloxy)-1,4-phenylenevinylene] (MEH-PPV) that exhibited negative differential resistance (NDR) function at room temperature. Although these seminal plastic NDR diodes are targeted for low power digital electronics, it is envisioned that modifications by materials replacements have the potential to form flexible tunneling junctions for multi-junction solar cells and offer higher flexibility and lower costs than their inorganic alternatives, such as silicon.

The focus of this current research work is to target this new application for highly transparent and low-resistance organic-based flexible tunneling diodes as a replacement for existing alternatives, which have lifetime issues related to metallic shorts and the inclusion of water-based materials. This work will streamline the

fabrication process of the tunneling diodes convolved with solar cell fabrication above and below it. Preliminary results for this research show that diodes substituting TiO_2 with MoO_3 and MEH-PPV with Copper Phthalocyanine (CuPc), do not indicate Zener tunneling behavior. This means that these materials, while excellent candidates, require further study to be utilized for this application. The potential benefits of this work are more efficient tunnel junctions for flexible, organic multi-junction solar cells that offer higher flexibility, manufacturability, lower costs, water-free, low-resistance with greater portability than their inorganic alternatives. At a deposition height of 43mm, which is measured from the top of the chamber.

Acknowledgements

I would like to express my deep appreciation to Dr. Paul R. Berger, Minjae Kim, and Conner Chambers for their continued support throughout this research experience. I also thank Nanotech West for the use of their facilities and resources. I would specifically like to thank Minjae Kim for spearheading evaluation of the different substrate-metal oxide films (XPS, UV-visible spectroscopy and IV-Testing).

Vita

2011……Texas Academy of Math and Science

2011 to present……..….B.S ECE, The Ohio State University

Fields of Study

Major Field: Electrical and Computer Engineering

Table of Contents

List of Tables

List of Figures

1. Introduction

There is a consumer need for point of use, flexible, organic solar cells that can be incorporated easily into electric automobiles, backpacks, coats, etc. as a portable energy source. Organic solar cells offer a flexible structure with lower costs than their inorganic alternatives, such as silicon. Multi-junction solar cells use multiple PN junction diodes in order to capture more sunlight than a single solar cell, each cell tuned to specific wavelengths. But, parasitic resistances are formed between these junctions, which decreases the efficiency of the solar cells. This work extends alternate flexible tunneling junctions for use in flexible multi-junction solar cells. Prior research by Professor Paul R. Berger's group at OSU demonstrated the feasibility of fabricating organic, polymer-based tunneling diodes using thin TiO_2 with MEH-PPV polymer[15]. Drawbacks to this approach are that high-temperature plasma oxidation was used after initial deposition of Ti to form the TiO_2 film. If this process were used in solar cell fabrication, the underlying polymers would denature. The objective of this project is to evaluate alternate materials that can be used in the fabrication of polymer tunneling junctions to further improve performance and streamline the fabrication process of tunneling diodes convolved with solar cell fabrication above and below it. The broader implications of this research are to fabricate flexible solar cells that are cheaper and more portable, serving to increase the use of solar cells as an alternative energy source.

1.1 Tunnel Diodes and Backwards Diodes

A typical tunnel diode, also known as an Esaki diode, operates on the principle of quantum tunneling, which states that electrons are able to pass through thin barriers due to the wave nature of the electron. Esaki Diodes are high speed, negative differential resistance (NDR) Devices that operate with current generated from carrier tunneling between energy bands constrained by the availability of energy states[14].

In a typical tunnel diode, an additional current component, generated by the quantum mechanical tunneling during energy band alignment, is added to the traditional diode current, whereby the tunneling current first increases with increased forward voltage, followed by a decrease, resulting in the vaguely N-shaped IV curve shown in Figure 1.

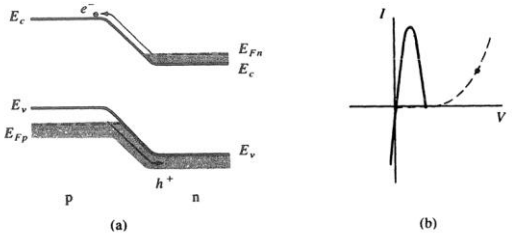

Band diagram (a) and *I–V* characteristic (b) for the tunnel diode beyond the tunnel current region. In (b) the tunneling component of current is shown by the solid curve and the diffusion current component is dashed.

Figure 1: Tunnel Diode Band Diagram and I-V Characteristic[14]

The forward bias of this I-V characteristic is known as negative differential resistance. Backwards diodes, have similar operation to a tunnel diode, but are doped less heavily, which attenuates the forward biased “hump” while maintaining the almost short circuit reverse Zener tunneling, resulting in different properties than an Esaki

diode[10]. One such difference is that, due to tunneling, a reverse-biased backwards diode has a similar IV characteristic to a forward-biased PN junction, albeit with very low voltage turn-on, as shown in Figure 2. Ideally there is no threshold voltage and the current immediately increases in reverse, starting at the origin. This property can be used to bypass harmful resistance caused by np junctions in multi-junction solar cells.

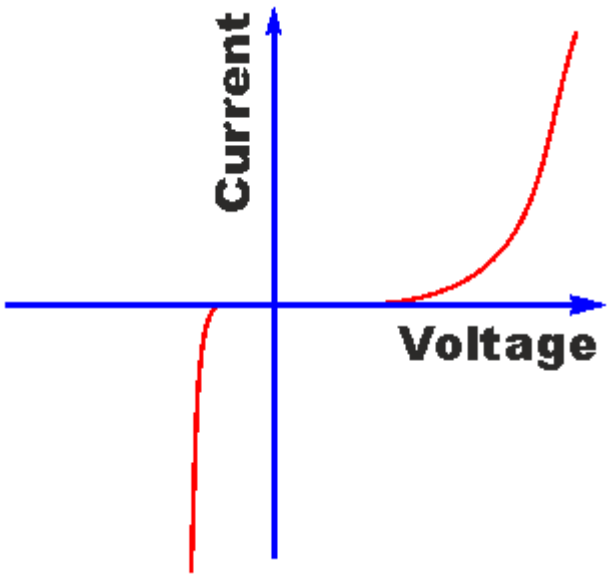

Figure 2: Backward Diode I-V Characteristic[10]

1.2 Conjugated Polymers

The first clearly defined conductive polymer was polyacetylene. Shirakawa *et al.* determined that, through doping with iodine and bromine, the conductivity of polyacetylene could be increased several orders of magnitude[8, 12].

Conductive polymers are often referred to as conjugated polymers and have a backbone that consists of alternating single and double bonds that opens up a forbidden energy gap, consistent with all semiconductors [8, 12]. Figure 3, below, displays the structure of several common types of conjugated polymers[8].

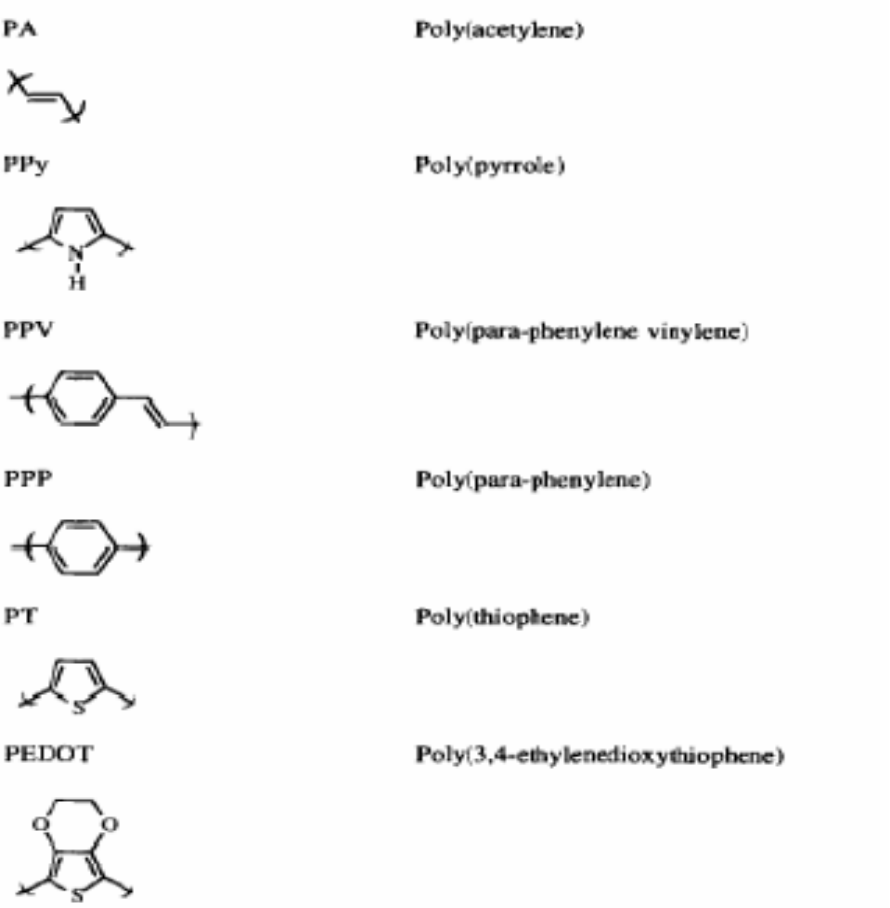

Figure 3: “Examples of Conjugated Polymers (adapted from Elsevier Science Resources)” [8]

The conductivity of these polymers is derived from the conjugated structure. The alternating single and double bonds allow for electron delocalization when electrons are added to or removed from the polymer backbone, which in turn allows for conduction[2]. Conjugated polymers have found applications in a number of fields, including photovoltaic devices and particularly organic light emitting diodes (OLEDs) represented on full-color displays on many mobile phones (i.e. Samsung, LG, etc.) and now some ultra-thin flat panel televisions [4]. They have drawn interest by their ultra-thin form factor, simplicity and Lambertian output for better off-axis viewability[11]. In photovoltaic

applications, they offer a lower cost alternative to fabrication of solar cells using inorganic materials such as silicon[4]. Conjugated polymers can be fabricated into thin films using room-temperature procedures[4]. This, in conjunction with their lower material costs, serves to decrease the manufacturing cost of organic solar cells[4]. The methods used to fabricate organic materials and the material properties, including increased flexibility, are also compatible with the processes required to fabricate large-area optoelectronic devices and electronic devices.

2. Previous Work

2. 1 Description of Previous Work

Professor Berger's group has developed and patented polymer tunneling diodes that could be utilized as low power memory[16]. The method described to create these diodes was the following: Indium tin oxide (ITO) coated glass substrates with a sheet resistance (Rs) below 10 Ω-cm. (A=0.19 cm^2) were used as substrates[16]. A thin layer of electron beam evaporated Ti metal (2-20 nm) was deposited. This layer was then oxidized using a high-temperature anneal with an oxygen plasma at an RF power of 80 W [16]. This oxidation process is known as plasma oxidation.

Following the plasma oxidation step, thin films of MEH-PPV were spin coated atop the TiO_2 layer from a 0.5% MEH-PPV solution in 80% toluene and 20% Tetrahydrofuran (THF) [16]. The devices were completed by a shadow mask evaporation of an Al cathode, which was about 250 nm thick [16]. The basic structure of the diode is shown in Figure 4, below.

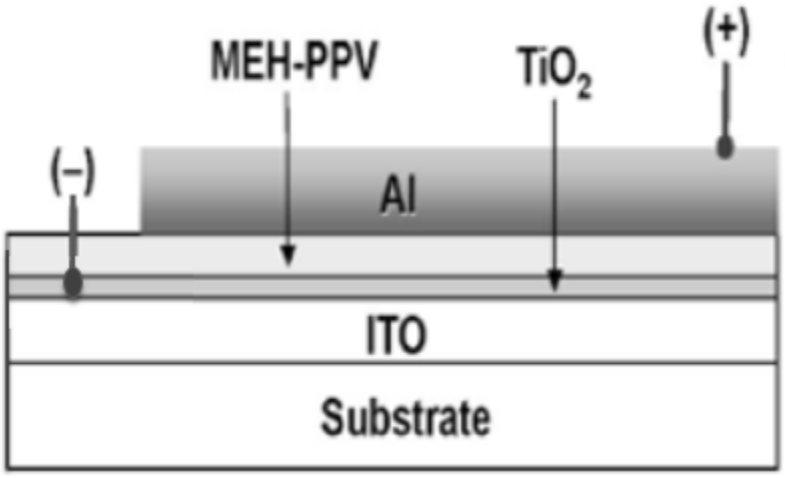

Figure 4: Diode Structure [16]

The J-V results of the polymer tunnel diode is shown in figure 5.

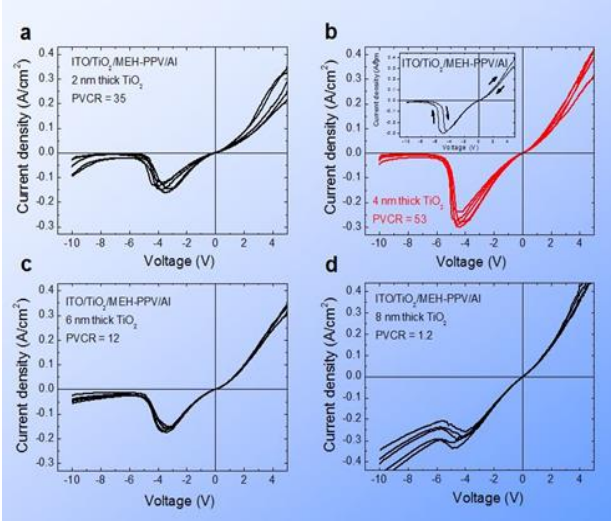

Figure 5: Diode J-V Characteristic [16]

These results suggested that the NDR behavior observed is due to tunneling through localized defect states that occur as a result of the plasma oxidation process used in the fabrication process of the TiO_2 films [16]. This theory was supported by J-V

data from diodes fabricated with TiO_2 films that underwent plasma oxidation at 400°C to achieve better crystallinity and displayed less significant NDR behavior [16].

2.2 Historical Context

Common approaches to interconnecting layers between subcells in organic tandem solar cells include thin metal layers and highly-doped PN junctions. The objective of the metal layers is to serve as a recombination center for the holes and electrons coming from the subcells and thereby create an ohmic contact between the subcells[17, 18]. The PN junctions interconnect the subcells by serving as recombination contacts to allow charge flow between subcells.[24]

In 1990, Hiramoto *et al*. used a thin Au layer to connect two identical cells and fabricate one of the first organic tandem solar cells[17, 19, 20]. An early study by Yakimov *et al*. in 2002 clearly showed that a thin layer of Ag could be used as an interlayer to provide a recombination site for holes and electrons and thereby create a series connection between subcells and lead to an addition of their photovoltages[17,19]. However, metal nanoclusters contact both P and N regions of the subcells and thus disallow selective hole or electron extraction, which has a detrimental impact on the potential efficiency of organic solar cells [17,23]. This is because using selective hole and electron extraction has been shown to increase charge transport in organic materials[23]. Therefore, using this method in organic solar cells would limit the efficiency of the devices and thereby restrict the potential use of the cells.

PEDOT: PSS is also frequently used in junctions to interconnect organic tandem cells due to its effectiveness as a P-type hole transport region [18, 21, 22]. Kawano *et al*., in

2006, was able to fabricate an organic tandem using an ITO/PEDOT:PSS junction[22]. However, PEDOT:PSS is acidic, which can degrade contacts over time and decrease device lifetime[17]. Also solution processing, the method by which PEDOT:PSS is typically deposited can cause damage to underlying subcells[18]. This is not an issue with thin metal layers, which are typically deposited by thermal evaporation and are more robust and can typically sustain subsequent solution processing for additional subcells[18].

Our approach utilizes Poly(3-hexylthiophene-2,5-diyl), or P3HT, and molybdenum trioxide(MoO_3) to fabricate a tunnel junction in order to bypass the inverse PN junction formed between subcells. This approach has the potential to increase the lifetime of these devices due to exclusion of water-based PEDOT: PSS, which decreases lifetime of the device by chemical degradation. Increased lifetime can also be achieved by avoidance of a thin metal layer, which reduces the efficiency of organic solar cells by causing shorts due to contact with both P and N regions of the subcells.

2.3 Differences from Previous Work

The current work differs from the previous in three key areas. These are application, materials used, and fabrication methods. These differences allow the current project to build upon work done previously and also to contribute new knowledge relating to the behavior and application of polymer tunneling diodes.

In terms of application, the previous work was used to fabricate digital electronics circuit elements, such as a monostable-bistable transition logic element (MOBILE) latch using polymer tunneling diodes connected in series [16]. The intended application for the

current work is to fabricate junctions to bypass high-resistance inverse p-n junctions, an n-p junction, in multi-junction solar cells.

Furthermore, while the previous diodes were fabricated using MEH-PPV and TiO_2, the junctions fabricated for the current research utilize alternate staggered band gap candidate materials for the metal oxide and organic layer in order to evaluate the behavior of these diodes as compared to the original and to evaluate their potential to fabricate tunneling junctions for use in multi-junction solar cells [16]. In fact, herein the key ingredient is the reverse Zener tunneling and not the forward biased NDR.

Moreover, the metal oxide layer for the original diodes was formed by metal evaporation of a pure metal followed by a high-temperature plasma oxidation process. If this process were used in solar cell fabrication, the underlying polymers in the solar cell would denature. In our current work, the metal oxide layer is fabricated using reactive sputtering. Because reactive sputtering does not include a high temperature process the underlying polymers would be unaffected in a solar cell fabrication process. Long-term, our end goal is to move to atomic layer deposition (ALD) that extolls atomic precision without a highly kinetic process that can be damaging. Sputtering is a facile way for a rapid materials down selection before jumping to ALD where a preferred chemical precursor will need to be identified.

3. Methodology

3.1 Overall Diode Fabrication Process

The fabrication process for the diodes used in this study is shown in Figure 6, below.

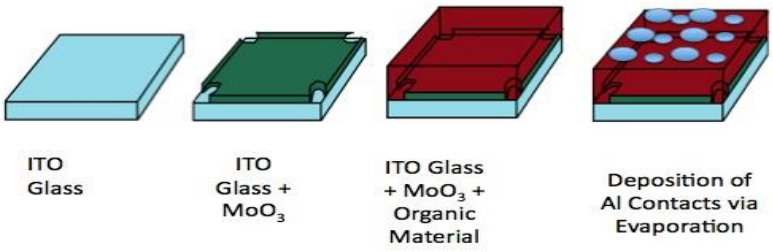

Figure 6: Diode Fabrication Process

The first step in the process is to clean the substrate material. For diode fabrication, the substrate used was ITO-coated glass (ITO glass). For characterization of the sputter-deposited metal oxide film, quartz or glass substrates were used. The metal oxide film used for this study was molybdenum trioxide(MoO_3).

Following the cleaning step, MoO_3 was sputter-deposited onto the substrate material to obtain a thickness of 1000Å, which is equivalent to 100nm.

After the MoO_3 sputtering process, the organic material was deposited. The organic material used in this study, Copper Pthalocyanine(CuPc), was deposited using organic evaporation. However, some organic materials can be deposition via a solution processing method known as spin-coating, which will be described later in section 3 as an alternative process.

The final step in the diode fabrication process is the evaporation of the metal contacts, which were aluminum. The contacts were deposited by a shadow mask evaporation process.

The individual steps described above are discussed in more detail in the remainder of Section 3.

3.2 Sample Cleaning

Quartz and glass samples are first rinsed in acetone to remove organic contaminants and then rinsed in isopropyl alcohol to remove acetone. The samples are then dried using a nitrogen gun. ITO-coated glass samples are first sonicated for five minutes in acetone, followed by a five-minute sonication in isopropyl alcohol, and then sonicated for five minutes in distilled water. The samples were then dried using a nitrogen gun.

a. b. c.

Figure 7: Sample Cleaning Tools, where (a) shows the separate beakers used for acetone, isopropyl, and DI Water when sonicating samples; (b) shows the equipment used for sonication; and (c) shows the nitrogen gun.

3.3 Deposition of Metal Oxide Films

The metal oxide films were deposited via reactive sputtering using the AJAX Orion Sputtering Tool at the Nanotech West Laboratory. The sputtering process deposits target material atoms on the substrate by the impingement of an inert gas plasma, typically argon, onto the target material. Figure 8, below illustrates this process visually showing how the argon ions impact the target material to remove atoms.

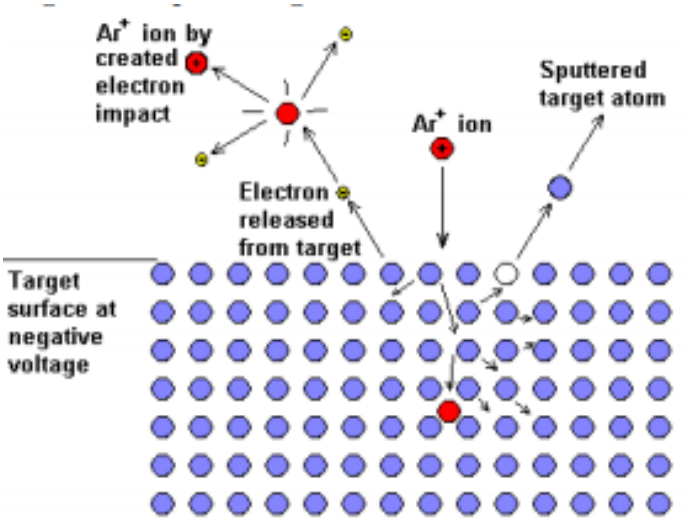

Figure 8: Sputtering Process[29]

The addition of O_2 gas into the chamber leads to the deposition of a metal oxide film, and this modified sputtering process is known as reactive sputtering.

An image of the sputtering tool used for this study is shown in Figure 9, below.

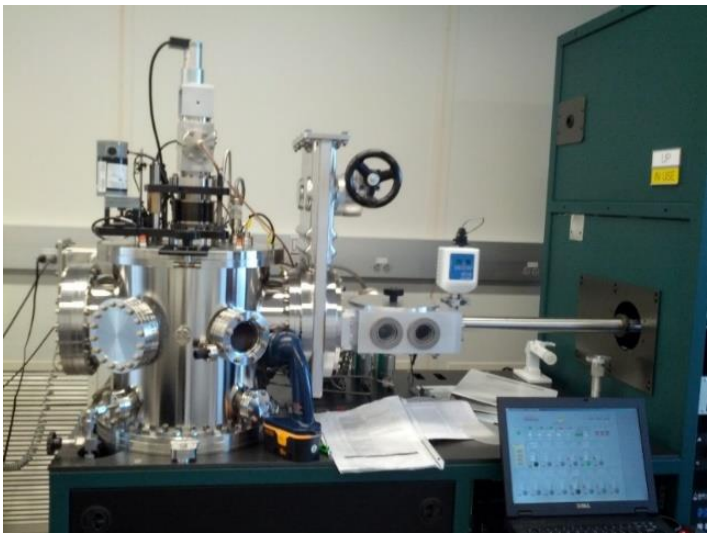

Figure 9: AJAX Orion Sputtering Tool.

The tool consists of a main chamber, where the depositions are performed and a small “load lock” chamber for loading and unloading samples. These chambers are separated via a gate that can be opened and closed, and the sample holder is moved between the chambers using a “loading arm”.

The target materials for deposition are located in the bottom of the main chamber in RF or DC guns, which are used to create the electric fields that allow the acceleration of the inert Ar gas onto the target materials. The sputtering tool at Nanotech West contains 2 DC guns and 3 RF guns for a total of 5 target materials. The setup of the target materials is shown in Figure 10. The main chamber also contains a crystal monitor to measure the deposition rate.

Figure 10: Sputtering Targets. [26]

Sample loading and unloading was done via a small load lock chamber because it is easier and faster to take a small chamber in and out of vacuum. The sample holder and the sample holder within the small load lock chamber are shown in Figure 11, below.

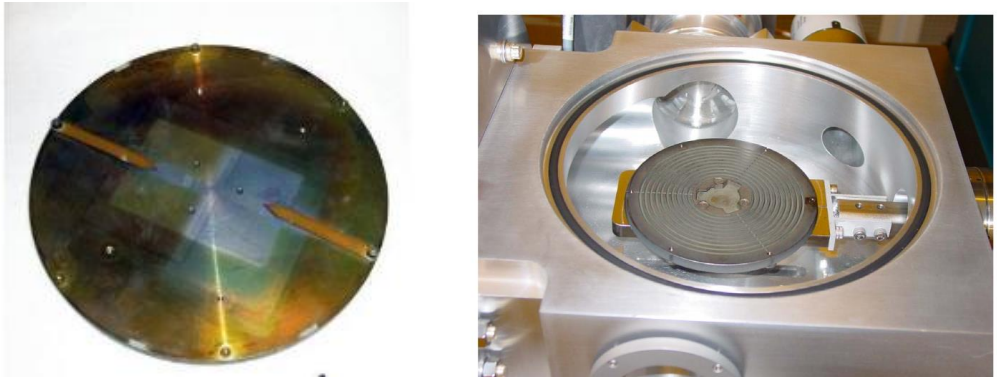

a. b.

Figure 11: AJAX Orion Sputter Tool Sample Holder a) bottom of the sample holder b) top of the sample holder within the load lock chamber[25,27]

The samples are mounted onto the bottom of the sample holder using pins. The samples are mounted on the bottom because the targets are located at the bottom of the chamber, and the samples have to be facing the targets for the deposition. Figure 11a shows a sample holder with 2 pins. The sample holder at Nanotech West had 4 pins and allowed 2 samples to be mounted at a time, using 2 pins for each sample to ensure stability.

For the sputtering tool used in this study, the recommended Argon gas flow is 20 standard cubic cm per minute (sccm) for a typical deposition in order to maintain plasma during deposition. The maximum allowed gas flow is 25 sccm total.

The tool settings are controlled via a software entitled Phase II provided by the tool manufacturer. Specifically, this software controls the sample rotation, substrate temperature, gas flows, pressure, target gun selection, and power applied to the target gun. This software is shown in Figure 12, below.

Labview based Computer Control on convenient slide-drawer

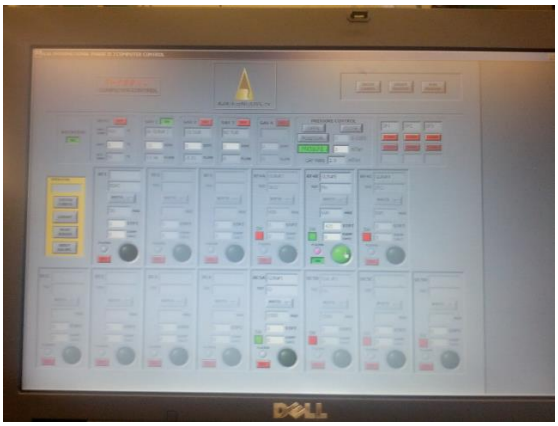

Figure 12: Phase II Software[26]

Prior to depositions a 10 minute pre-clean, or pre sputter, is done using the target material to ensure that the main chamber is free of contaminant material from prior depositions. This is done by performing a deposition at the same settings as the actual deposition with no samples present. During the pre-sputter process an empty sample holder is loaded into the chamber to ensure that the top of the main chamber does not get coated.

In order to accurately measure the deposition rate of the target material, a crystal monitor is placed at the deposition height of the samples, 43mm from the top of the chamber. Due to the design of the sputter tool, the crystal monitor is out of the way during the actual deposition. So, the deposition rate is measured during the pre-clean step.

Parameters for deposition are 420W applied to the RF gun, 25 rpm rotation of the sample holder to ensure an even coating, and a pressure of 3 mTorr. The target material for this study was Molybdenum, and Argon and Oxygen gas flows were varied in order to obtain the required oxide. The sputter deposited Molybdenum Oxide films were 1000Å, which is equivalent to 100nm, for all samples.

3.4 Deposition of Polymer Films

Polymer films were deposited by either organic evaporation or spin-coating. Spin-Coating is a thin film deposition process where polymer solutions are deposited on samples that are rotated at high speeds in order to create a thin polymer film on the sample. The concentration of the polymer solution and the speed of rotation can be modified to produce the polymer film required for a given application. Due to the light

and air sensitivity of the polymer films, spin-coating took place within a glove box with an inert nitrogen atmosphere. A spin coating tool is shown in Figure 13.

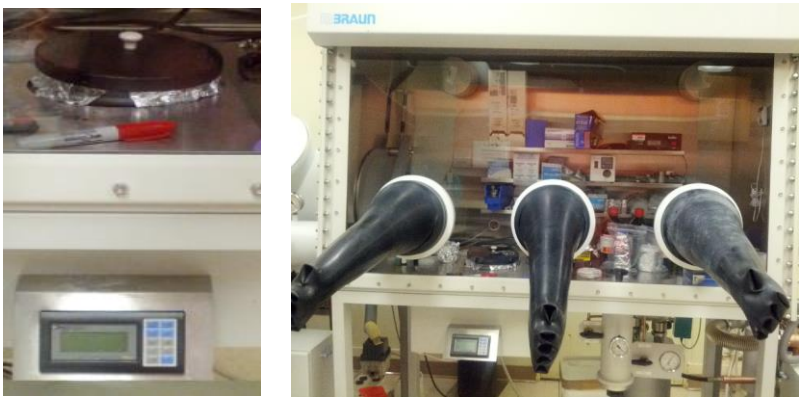

a. b.

Figure 13: Spin-Coater Equipment, where (a) shows controls for the spin-coater. (b) shows MBraun glovebox containing the spin-coater for depositing P3HT.

An organic vapor deposition process involves the thermal sublimation of an organic compound into a vapor stream and subsequent condensation of the compound onto the sample material[1]. This process has the advantages of decreased waste and uniform coating of the organic compound [1].

An example of an organic evaporator is shown in Figure 14.

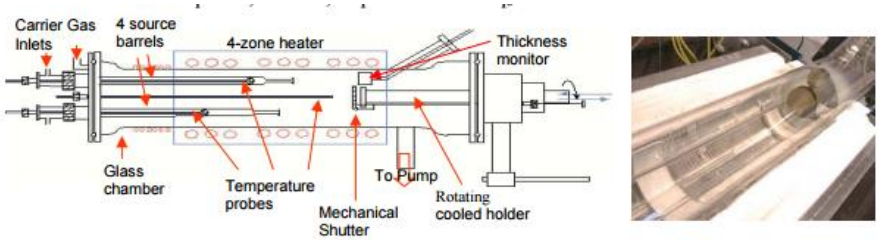

Figure 14: Organic Evaporator [1]

3.5 Contact Deposition

Aluminum contacts were deposited using shadow mask evaporation, which involves thermal evaporation and subsequent condensation of the aluminum onto the sample material through a mask. An evaporator is shown in Figure 15, below.

Figure 15: Edwards evaporator system inside MBraun glovebox for deposition of final cathodes.

3.6 Characterization of Oxide Films

3.6.1 Ultraviolet Visible Spectroscopy

UV-Vis Spectroscopy can be used to measure the transmission of light in the UV and visible spectra. It measures the intensity of light before and after it enters a sample and calculates the transmittance using the formula [9]

$$T = I/I_0$$

Percentage transmittance can also be calculated using the formula[9]

$$\%T = 100(I/I_0).$$

3.6.2 X-ray Photoelectron Spectroscopy

X-ray photoelectron spectroscopy (XPS) is a surface characterization method that makes use of the photoelectric effect to analyze the electronic structure of a material[3]. The photoelectric effect describes the electronic emission of a material after being exposed to electromagnetic radiation. This can be simply described by the formula

$$KE = h\nu - BE - \phi_s$$

In this formula, *KE* is the kinetic energy of the electron, *BE* is the binding or ionization energy of the electron, *h* is Plank's constant, ν is the frequency of the emission, and ϕ_s is the work function of the spectrometer [15]. The ionization energy of the emitted electron is related to its electron orbital. XPS makes use of this information by exposing the sample material to x-rays in an ultra-high vacuum in order to avoid electron scattering by gas particles. The emission spectrum is then analyzed to determine what electron orbitals are present and thus, what elements are present in the sample. The shifts in KE, rigid shifts in the spectra, and angle dependence can also be used to identify chemical bonding environments and band bending [15].

For this study, XPS tests were performed on the deposited Molybdenum Oxide films to verify the oxidation state. The XPS source was a monochromatic aluminum source and the tests were performed at a standard voltage of 12kV and a current of 10mA. The Mo 3d orbital level gives rise to a doublet of 5/2 and 3/2, and the Mo3d 3/2 and Mo 3d 5/2 peaks both have different binding energies. Therefore, XPS verified the oxidation state by examination of the Mo3d 3/2 and Mo 3d 5/2 peaks. Peak fitting was done by CASA XPS software where the raw XPS data was first processed by

elimination of noise signal. Following this spin orbit splitting between Mo 3d doublet core levels was performed where the difference between the peaks was given by

$$\Delta = \text{Mo 3d 3/2} - \text{Mo 3d 5/2} = 3.13 \text{ eV}$$

Additionally, the peak area ratio was given by

$$\text{Mo 3d 3/2: Mo 3d 5/2} = 2:3$$

The final step in the peak-fitting process was charge compensation by C 1s peak(284.5eV).

Reference Values for the MoO_3 3d peak are shown in Table 1, below.

Table 1: Reference values for Mo 3d peak[24]

Reference

Mo state	Mo 3d 5/2 (eV)	Standard deviation
Mo (0)	227.8	0.5
Mo (4+) : MoO_2	229.7	0.9
Mo (5+) : Mo_4O_{11}	231.1	
Mo (6+) : MoO_3	**232.6**	**0.2**

3.7 J-V Characterization

J-V testing was used to electrically characterize the completed diode samples. The J-V testing station, shown in Figure 16, was used to apply a range of voltages and measure the resultant current density. The resultant plot was used to analyze the electrical behavior of the sample.

Figure 16: J-V Testing Equipment

3.7 Material Determination

Minjae Kim, a graduate student in Dr. Berger's lab group created an energy diagram of potential materials to fabricate the tunnel diodes, which is shown in Figure 17. The metal oxides and conjugated polymers should exhibit a staggered junction in order to be used for a tunneling diode. Thus, from Figure 17, it appears that Molybdenum Oxide (MoO_3), Tungsten Oxide (WO_3), and Vanadium Oxide (Va_2O_5) are particularly promising due to the staggered energy levels between these materials and the candidate conjugated polymers.

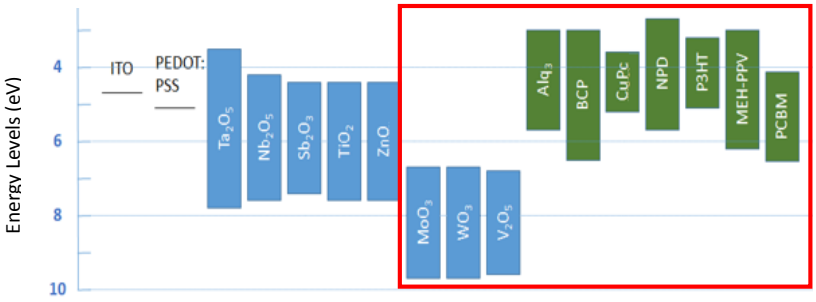

Figure 17: Candidate materials for staggered bandgap Zener tunnel junctions.

To this end, thin films of Molybdenum Oxide were reactively sputtered onto glass and quartz samples using the AJA Orion Sputter tool at Nanotech West Laboratory. The deposition rate was measured, using a crystal monitor, to be 1.4A/s at RF power of 420W. Copper phthalocyanine (CuPc) was chosen as the organic material because it can be deposited by organic vapor deposition, which offers a more accurate thickness measurement than is available for spin-coated films.

4. Results

Molybdenum Oxide was initially deposited using an Argon gas flow of 15 sccm and an Oxygen gas flow of 5 sccm, 25% O_2 partial pressure. These samples, which are shown in Figure 18, are not translucent.

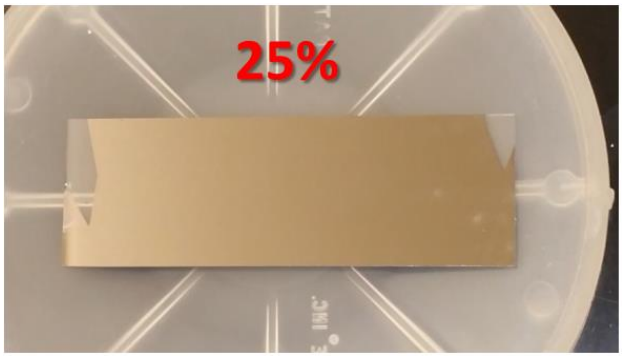

Figure 18: Molybdenum Oxide on glass substrate deposited at 25% O_2 partial pressure

This property is detrimental to the use of these film in photovoltaic applications which require transmission of light to underlying layers.

Additionally, the resultant XPS curves for the Molybdenum Oxide samples deposited with 25% O_2 are shown in Figure 19. The blue curve represents the Mo 3d

5/2 peak, and the red curve represents the Mo 3d 3/2 peak. Comparison with the reference values in Table 1 indicate that the oxide deposited was the Mo(5^+) state, which corresponds with MoO_2 rather than MoO_3.

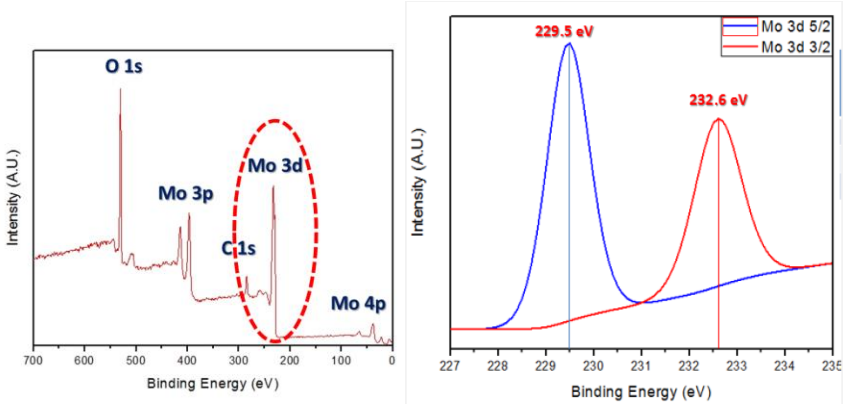

a b

Figure 19 : XPS results for sputter-deposited films at 25 % oxygen partial pressure. (a) shows complete results. (b) dispays closeup on the Mo3d peak.

The staggered junction diagram in Figure 17 indicated that MoO_3 was a good candidate for these diodes. However, the sputtering process was depositing MoO_2 film. Therefore, it was concluded that a higher oxygen partial pressure was needed to promote the deposition of MoO_3 films via sputtering.

Because of this, molybdenum oxide layers were deposited via sputter deposition at 40%(15sccm Ar/ 10sccm O_2), 50%(10sccm Ar/ 10sccm O_2), 60%(10sccm Ar/ 15sccm O_2), and (5sccm Ar/ 20sccm O_2), 80% O_2 partial pressure. Samples deposited at 40% and 50% partial pressure were also deposited with, and without, substrate heating at 100^{o}C to determine whether heat applied during deposition would promote the formation of MoO_3 films through a higher oxidative state.

From Figure 20, below, it was apparent that the translucency of the films increased with oxygen partial pressure, which is a property that is beneficial to photovoltaic applications for reasons stated earlier in this section.

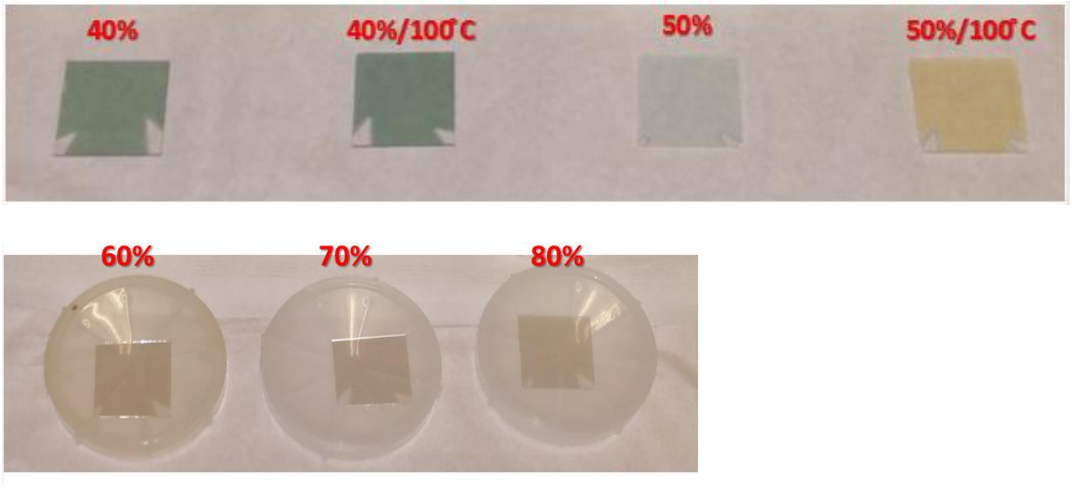

Figure 20: Molybdenum Oxide Deposited at various O_2 partial pressures

Ultraviolet Visible Spectroscopy (UV-Vis) results for samples deposited with 40% and 50% O_2 partial pressures, as shown in Figure 21, indicates that 50% O_2 partial pressure during sputter deposition results in films with higher optical transmission than films deposited at 40% O_2 partial pressure.

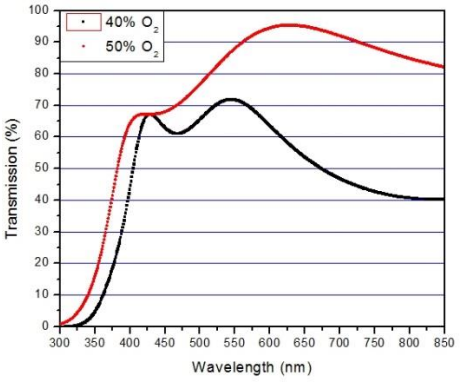

Figure 21: UV-Vis Results

The XPS results for the Molybdenum oxide samples deposited at all tested oxygen partial pressures are shown in Figure 22.

Measured

Oxygen partial pressure (%)	Substrate heating	Mo 3d 5/2 (eV)	Mo 3d 3/2 (eV)	Mo state
25	X	231.1	232.6	5+
40	X	232.8	235.9	**6+**
40	100°C	232.7	235.8	**6+**
50	X	232.6	235.7	**6+**
50	100°C	232.9	236.0	**6+**
60	X	232.8	235.9	**6+**
70	X	232.6	235.7	**6+**
80	X	232.7	235.8	**6+**

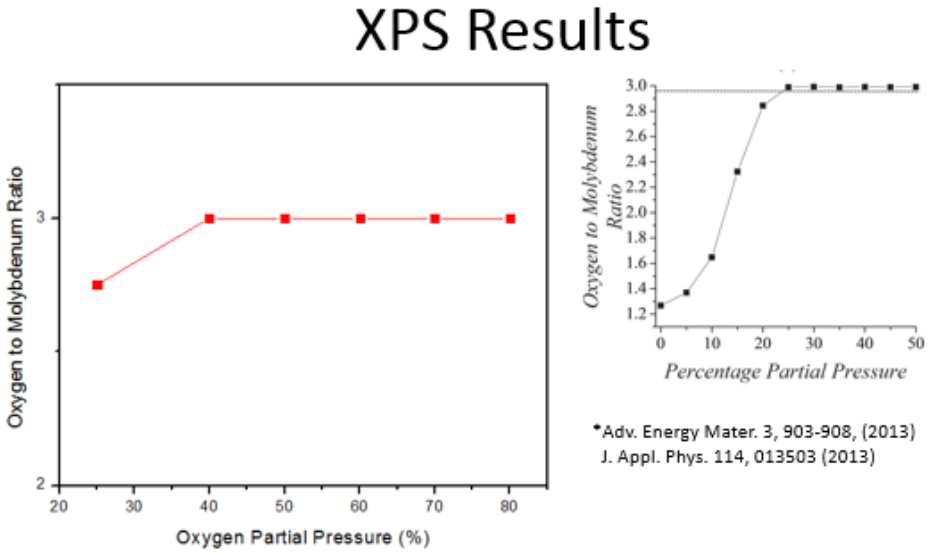

Figure 22: XPS Results deposition[8,13]

However, as indicated in Figure 23, the deposition rate decreases significantly as oxygen partial pressure increases. In order to balance this, and oxygen partial pressure of 40%, without substrate heating, was chosen to deposit the molybdenum oxide layer.

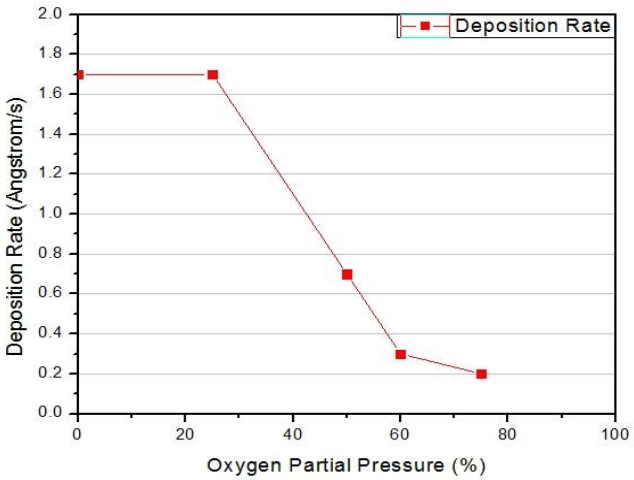

Figure 23: Deposition Rate vs O_2 Partial Pressure

J-V results for diodes are shown in Figure 24. For these measurements, the ITO anode was connected to negative electrode and the aluminum cathode was connected to the positive electrode.

J-V Result

Device Structure: ITO/MoO_3(100nm)/CuPc(10nm)/

Current Density Scale: 0.1 A/cm^2

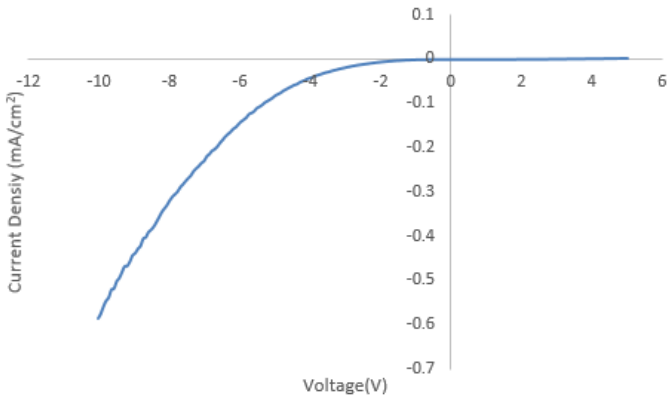

25% Oxygen Partial Pressure

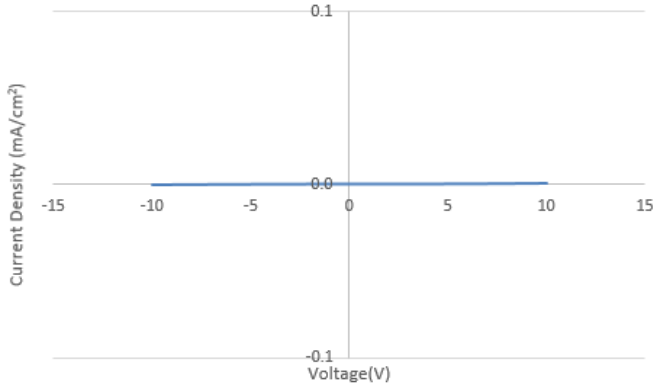

40% Oxygen Partial Pressure

	25%	40%
Current density @ -1 V	$-5.0x10^{-4}$	$-2.0x10^{-5}$
Current density @ +1 V	$7.4x10^{-5}$	$-5.2x10^{-6}$

Figure 24: J-V Results for diodes fabricated using Molybdenum Oxide deposited at 25% and 40% O_2 partial pressure.

J-V Result

Device Structure: ITO/MoO_3(100nm)/CuPc(10nm)/

Current Density Scale: 0.0001 A/cm^2

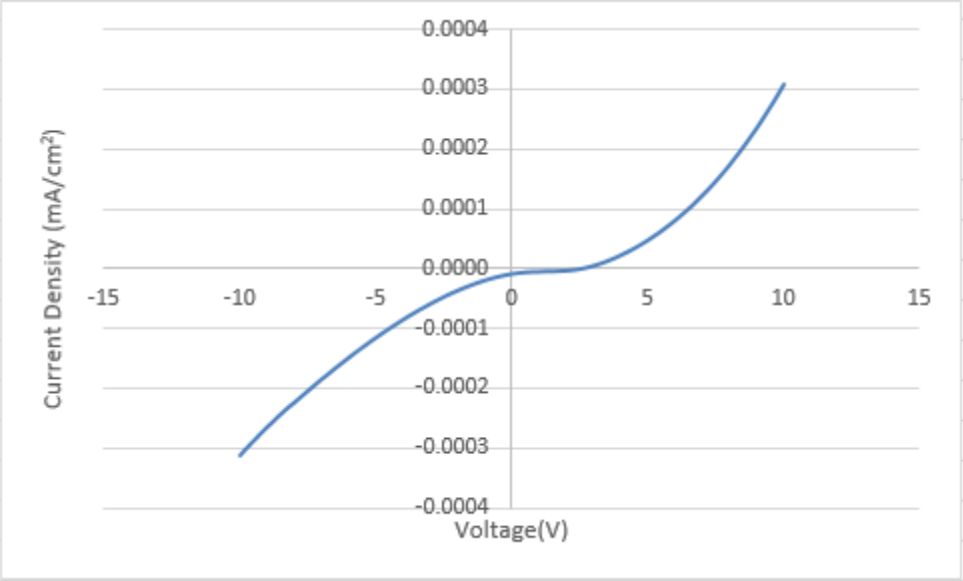

Figure 25: Rescaled J-V Results: 40% oxygen partial pressure

The results for the diodes fabricated with MoO_3 films deposited at 25% O_2 partial pressure and diodes fabricated with MoO_3 films deposited at 40% O_2 partial pressure are plotted using a current density scale of 0.1 mA/cm^2 for comparison. In order to view the data for the diodes fabricated with MoO_3 films deposited at 40% O_2 partial pressure more clearly, the data was rescaled using a current density scale of 0.0001 mA/cm^2, which is displayed in Figure 25. In order to bypass resistive NP junctions, there should ideally be no threshold voltage with the current immediately increasing in reverse, starting at the origin. From the data displayed in Figure 24 and Figure 25, no significant tunneling behavior is observed for either the diodes fabricated at 25% O_2 partial pressure or for the diodes fabricated with a Molybdenum Oxide layer deposited at 40%

O_2 partial pressure. While there is significant reverse current in the diodes fabricated at 25% O_2 partial pressure, given that the current increases substantially after -5V, there may be some contribution from avalanche breakdown.

5. Future Work

Future work could include performing additional characterization of the Molybdenum Oxide film. For example, Atomic Force Microscopy(AFM) could be used to determine surface roughness and potential gaps in the Molybdenum Oxide surface that would allow the ITO anode to contact the organic material and cause shorts. Other work could be to alter the thickness of the CuPc and MoO_3 layers to improve the performance of the completed diode. Alternative materials for the organic and metal oxide layers could also be selected to improve diode performance.

For example, P3HT is a material that is commonly used in solar cells as a donor material [5]. Figure 17 indicates that P3HT exhibits a good staggered junction with MoO_3. Figure 26 displays the energy diagram, P3HT structure, and structure of a diode fabricated using P3HT and MoO_3.

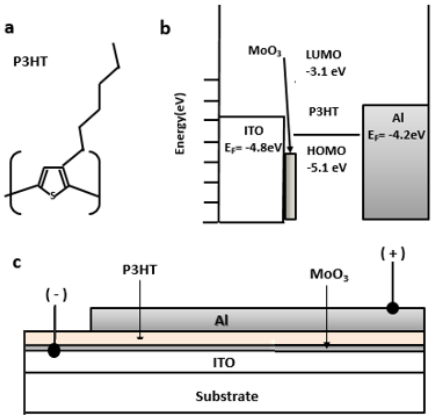

Figure 26: MoO3/P3HT junction

This information indicates that while this junction will not have NDR, it may be a good candidate material for backwards diodes to use in multi-junction solar cells because of the staggered energy levels exhibited by MoO_3 and P3HT.

Another potential organic candidate material for the junctions is PBDTTT-C. It is an air and light sensitive, low bandgap material that was first introduced by Solarmer with the University of Chicago. However, PBDTTT-C uses solvents rather than annealing for morphology control, which is beneficial to create a more streamlined fabrication method for Zener tunneling junctions for multi-junction solar cells.

Furthermore, following the fabrication and testing of potential tunneling junctions, complete solar cells could be fabricated in order to test whether the junctions are behaving as predicted. Further work could also be done to optimize the fabrication of the junctions convolved with solar cell fabrication above and below it.

6. Conclusions

Diodes were fabricated using Molybdenum Oxide and CuPc. Diodes fabricated with 100nm of Molybdenum oxide sputter-deposited at 25% and 40% O_2 partial pressure did not show significant Zener tunneling in their IV characterization.

Therefore, further characterization is needed to determine why these diodes do not display Zener tunneling. One possible reason could be the thickness of the molybdenum oxide and CuPc layers. Future work could include fabricating and testing diodes with thinner layers of MoO_3 and CuPc. Other materials could also be used to fabricate the diode, including PBDTTT-C, a conductive polymer that allows morphology

control with solvents added prior to spin-coating [5]. This may produce a better organic conductive layer and allow improved carrier flow in the completed diode. P3HT, a conductive polymer often used as a donor material in solar cells, displays a staggered band structure with a MoO_3 layer and is a good candidate for backwards diode to connect multiple PN junctions in tandem solar cells.

7. References

1. J.B Benziger and S. Forrest. “Organic Vapor Phase Deposition for Optoelectronic Devices.” Internet: http://www.princeton.edu/~benziger/OVPD.pdf, 2004 [Aug. 25, 2015].

2. C. J. Brabec, V. Dyankonov, and U. Scherf.*Organic Photovoltaics Materials, Device Physics, and Manufacturing Technologies*. Weinheim: Wiley-VCH, 2008.

3. L.J.Brillson, *Surfaces and Interfaces of Electronic Materials*. Weinheim: Wiley-VCH, 2010, 570 pages.

4. W. Cao., and J. Xue. "Recent Progress in Organic Photovoltaics: Device Architecture and Optical Design." *Energy & Environmental Science*, vol. 7, pp.2123-2144, Mar. 2014.

5. H.Chen, J. Hou, S. Zhang, Y. Liang, G. Yang, Y. Yang, L. Yu, Y. Wu, and G. Li. “Polymer solar cells with enhanced open-circuit voltage and efficiency.” *Nature Photonics*, vol. 3, pp. 649-653, 2009.

6. C.S Fadley, “X-ray photoelectron spectroscopy: Progress and perspectives”. *Journal of Electron Spectroscopy and Related Phenomena,* vol. 2, pp. 178–179, Feb. 2010

7. .J. Griffin, D.C. Watters, H. Yi, A. Iraqi, D. Lidzey, and A.R. Buckley. “The Influence of MoOx Anode Stoicheometry on the Performance of Bulk Heterojunction Polymer Solar Cells.” *Advanced Energy Materials,* vol. 3, pp. 903-908, Apr. 2013.

8. M.H Harun, E. Saion, A. Kassim, N. Yahya, and E. Mahmud. "Conjugated conducting polymers: A brief overview*." UCSI Academic Journal: Journal for the Advancement of Science & Arts 2*, pp. 63-68, Jan, 2007.

9. T.Owen. *Fundamentals of UV-visible Spectroscopy*. n/a: Hewlett-Packard Company, 1996.

10. I. poole. “Backward Diode Tutorial”. Internet: http://www.radio-electronics.com/info/data/semicond/tunneldiode/backward-diode.php , [Aug. 25 2015].

11. J. Shinar and R. Shinar. "Organic Light-emitting Devices (OLEDs) and OLED-based Chemical and Biological Sensors: An Overview." *Journal of Physics D: Applied Physics*, vol. 41, pp. 133001, Jun. 2008.

12. H. Shirakawa, E.J. Louis, A.G. Macdiarmid, C.K. Chiang, and A.J. Heeger.

"Synthesis of Electrically Conducting Organic Polymers: Halogen Derivatives of Polyacetylene, (CH) X." *Journal of the Chemical Society, Chemical Communications*, pp. 578, Jan. 1977

13. H. Simchi, B.E Mccandles, T. Meng, J.H. Boyle, and W.N Shafarman, "Characterization of reactively sputtered molybdenum oxide films for solar cell application". *Journal of Applied Physics.* vol. 114, pp. 013503. Jul. 2013

14. B.G. Streetman and S.K. Banerjee, *Solid State Electronic Devices*, Upper Saddle River, NJ :Prentice Hall, 2006. 608 pages

15. C. D. Wagner. , W. M. Riggs , L. E. Davis , J. F. Moulder, and G. E. Muilenberg: *Handbook of X-ray Photoelectron Spectroscopy,* Eden Prairie, MN: Perkin-Elmer Corp*,* 1979, 190 pages.

16. W. Yoon, S. Chung, P.R. Berger, and S.M. Asar. "Room-temperature Negative Differential Resistance in Polymer Tunnel Diodes Using a Thin Oxide Layer and Demonstration of Threshold Logic." *Applied Physics Letters* , vol. 87, pp. 203506,. Nov. 2005

17. Sista S, Hong ZR, Chen LM, Yang Y. Tandem polymer photovoltaic cells—current status, challenges and future outlook. Energy EnvironSci 2011;4:1606–20.

18. You, Jingbi, Letian Dou, Ziruo Hong, Gang Li, and Yang Yang. "Recent Trends in Polymer Tandem Solar Cells Research." Progress in Polymer Science 38.12 (2013): 1909-928. Web.

19. Yakimov A, Forrest SR. High photovoltage multiple-hetero junction organic solar cells incorporating interfacial metallic nanoclusters.Appl Phys Lett 2002; 80:1667–9.

20. M. Hiramoto, M. Suezaki and M. Yokoyama, Chem. Lett., 1990, 327.

21. J. Drechsel, B. Mannig, F. Kozlowski, M. Pfeiffer, K. Leo and H. Hoppe, Appl. Phys. Lett., 2005, 86, 244102.

22. Kawano K, Ito N, Nishimori T, Sakai J. Open circuit voltage of stacked bulk heterojunction organic solar cells. Appl Phys Lett 2006;88,073514/1–3.

23. Lee, Ju Min, Ji Sun Park, Sun Hwa Lee, Hoyeon Kim, Seunghyup Yoo, and Sang Ouk Kim. "Selective Electron- or Hole-Transport Enhancement in Bulk-Heterojunction Organic Solar Cells with N- or B-Doped Carbon Nanotubes." *Adv. Mater. Advanced Materials* 23.5 (2010): 629-33.

24. "X-ray Photoelectron Spectroscopy (XPS) Reference Pages." *: Molybdenum*. XPS Fitting, Oct. 2009. Web. 05 Nov. 2015.

25. "AJA ORION SPUTTER TOOL." *AJA Orion Sputter*. UTDallas, n.d. Web. 05 Nov. 2015.

26. "ATC Orion Series Sputtering Systems." AJA International. N.p., n.d. Web. 07 Nov. 2015. <http://www.ajaint.com/atc-orion-series-sputtering-systems.html>.

27. "Nano3 Cleanroom." Nano3 Cleanroom. California Institute for Telecommunications and Information Technology, n.d. Web. 07 Nov. 2015. <http://nano3.calit2.net/>.

28. Kirschbrown, Justin. "RF/DC Magnetron Sputtering." (n.d.): n. pag. The University of North Carolina at Chapel Hill, 20 Nov. 2007. Web. 8 Nov. 2015.